Available online at www.sciencedirect.com
ScienceDirect
International Journal of Heat and Mass Transfer 49 (2006) 4762–4772
International Journal of HEAT and MASS TRANSFER
www.elsevier.com/locate/ijhmt

Analysis of moisture flow in porous materials using microfocus X-ray radiography

Staf Roels *, Jan Carmeliet

Laboratory of Building Physics, Katholieke Universiteit Leuven, Kasteelpark Arenberg 40, B-3001 Leuven, Belgium

Received 18 October 2005; received in revised form 25 April 2006
Available online 1 September 2006

Abstract

Microfocus X-ray projection is presented as an accurate experimental technique for measuring moisture transport processes in porous materials. The technique has evolved from the better-known medical technique. Compared to classical γ-ray and NMR-techniques it allows an instant and accurate determination of the two-dimensional transient moisture content profiles. A calibration procedure is presented to optimise the resolution in moisture content by choosing an adequate sample thickness in relation to the energy of the X-ray source. To illustrate the capabilities of the X-ray projection method, examples of two-dimensional liquid water uptake in homogeneous, heterogeneous, micro- and macro-fractured materials are presented.

Keywords: X-ray; Moisture content; 2D profiles; Porous media

1. Introduction

The measurement of moisture content distributions for the study of liquid transport in porous materials is of crucial relevance in several disciplines: hydrology, soil science, geology, buildings physics, biomechanics... In the last decades, advanced experimental techniques have been developed to determine transient liquid water profiles in a non-destructive way. Well-known are the γ-ray attenuation technique [1–3] and the NMR- [4,5] and MRI-technique [6,7]. Most of those techniques are in essence one-dimensional techniques, i.e. each point is scanned at a given moment of time and thus a moisture content profile at a certain time can only be determined by interpolation in the time domain. A fast and very potential alternative to visualise fluid flow in porous materials is neutron tomography (e.g. Masschaele et al. [8]). Major drawback of the latter is the extremely high investment cost, making neutron tomography hardly available.

Recently, also the X-ray attenuation technique is applied to analyse flow in porous materials. Cadoret et al. [9] used X-ray computer tomography to visualise porosity and equilibrium fluid distributions in limestone. The porosity map was obtained by subtraction of the fully water saturated image from the dry rock image. Subtraction of the image of a rock at a given fluid saturation from the fully saturated image gives an image of the gas content. Tidwell et al. [10] used X-ray imaging for determining two-dimensional tracer concentration fields during a diffusion test in rock. Akin et al. [11] developed a CT-compatible imbibition cell to study water imbibition into diatomite samples.

In this paper, we use microfocus X-ray projection for the analysis of transient two-dimensional liquid water flow in porous materials. A quantitative moisture content map at a given time is obtained by subtraction of a reference image (e.g. image of the dry sample) from an image taken during moisture transfer. Special attention is given to the optimisation of the measurement method in order to obtain a high resolution in space, time and moisture content. We illustrate the applicability of the X-ray projection method for analysing liquid water uptake processes in

* Corresponding author. Tel.: +32 16 321349; fax: +32 16 321980.
E-mail address: staf.roels@bwk.kuleuven.be (S. Roels).

0017-9310/$ - see front matter © 2006 Elsevier Ltd. All rights reserved.
doi:10.1016/j.ijheatmasstransfer.2006.06.035

Nomenclature

a, b	coefficients
d	thickness of the object
D	liquid water diffusivity
E	(X-ray) energy
I	intensity of X-ray
L_1	source to object distance
L_2	object to detector distance
l_s	spot size of the source
M	magnification, $1 + L_2/L_1$
n	number of pixels
R_d	resolution of the camera
R_w	moisture content resolution
R_x	spatial resolution
s	variation
t	time
V	volume
w	water content
x, y	coordinates
Z_e	effective atomic number

Greek symbols

λ	Boltzmann variable
ρ	density
μ	attenuation coefficient

Subscripts

B	boundary
ef	effective (attenuation coefficient)
opt	optimal
w	liquid water
0	incident (energy)

homogeneous, heterogeneous, micro- and macro-fractured porous materials. The validity of the one-phase diffusion approach for describing water uptake processes is evaluated using the Boltzmann transformation method.

2. X-ray radiography

2.1. Main principles

X-ray radiography can be used to characterise in a non-destructive way the internal features of non-transparent materials. When an object is irradiated with an X-ray beam, the X-rays attenuate due to the interaction with the material. For monochromatic X-rays, the relationship between the incident and attenuated X-rays (I_0 and I respectively) is expressed by Beer's Law [12]:

$$\frac{I}{I_0} = \exp(-\mu d) \tag{1}$$

where μ is the attenuation coefficient and d is the length of the X-ray path through the object (i.e. the thickness of the object). For energy levels below 200 keV, attenuation depends mainly on two processes: photoelectric absorption and compton scatter. The attenuation coefficient can be expressed as [13]:

$$\mu = \rho\left(a + b\frac{Z_e^{3.8}}{E^{3.2}}\right) \tag{2}$$

with ρ the bulk density of the material, Z_e the effective atomic number of the material [14], E the X-ray energy and a and b are the energy-dependent coefficients.

2.2. X-ray apparatus and method applied

This study is performed on an AEA microfocus X-ray apparatus. Microfocus X-ray projection is based on the same principles as the classical medical technique, but here the X-ray source has a much smaller spot size (around 10 μm) which allows placing the object near the X-ray source and capturing X-ray radiographs of the object with a primary magnification, enhancing the spatial resolution. The maximum X-ray source energy of the apparatus used for this study is 160 keV. The apparatus is equipped for computer tomography, but in this study we limit to X-ray photography on plates of porous materials and no rotation of the samples is performed. Because the plates are positioned perpendicular to the X-ray beam, as illustrated in Fig. 1, one single measurement provides us with a two-dimensional picture of the plate. Luminescent screens are used to convert the X-rays into light photons. The detector for light photons is a CCD 12-bit camera (4096 intensity levels) that visualises intensity levels as greyscales. The size of the greyscale images is 1024 × 1024 pixels. The real-time images are digitised and corrected for spatial distortion and scatter [13]. To reduce noise, several pictures are averaged at a speed of 25 frames/s. We used an averaging of 256 frames, which results in a time resolution of 10 s for one image.

2.3. Spatial resolution R_x

For an infinitesimal thin plate, the spatial resolution is determined by the spot size of the X-ray source l_s, the resolution of the detection system R_d and the magnification M [15]:

$$R_x = \frac{R_d}{M} + \left(1 - \frac{1}{M}\right) l_s \tag{3}$$

The resolution of the detector R_d equals the geometric size of a pixel on the detector. The magnification is determined by the source-to-object distance L_1 and object-to-detector distance L_2, or $M = 1 + L_2/L_1$. Eq. (3) states that the resolution increases when the object is placed closer to the source. For a specimen with a certain thickness, however,

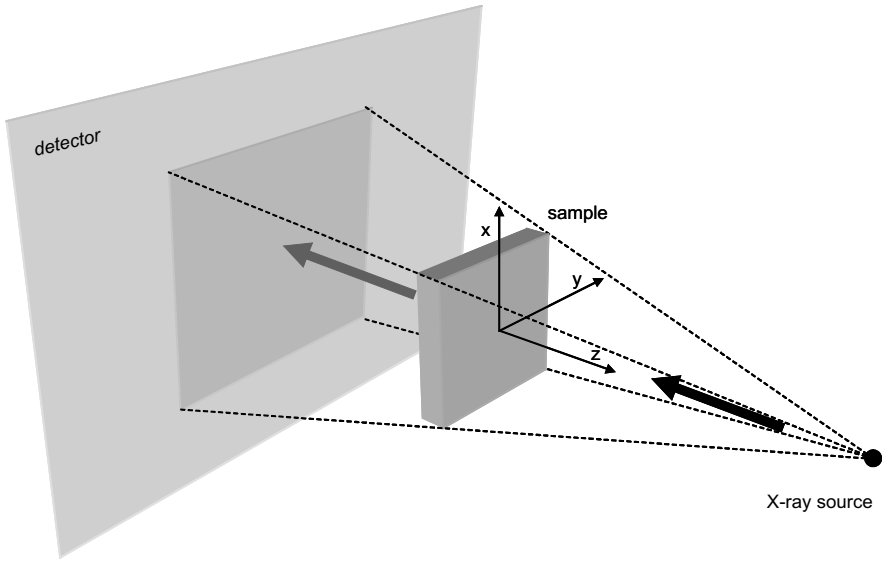

Fig. 1. Schematic overview of the experimental set-up of the X-ray projection method.

Eq. (3) is only valid in the centre of the X-ray beam. Away from the centre, the thickness of the plate will smooth out jumps in attenuation, reducing the spatial resolution. This effect can clearly be illustrated at the edge of a sample where the jump from the attenuation coefficient of the material to the attenuation coefficient of the air is smoothed out in the so-called edge-response function (ERF) (see inset of Fig. 2).

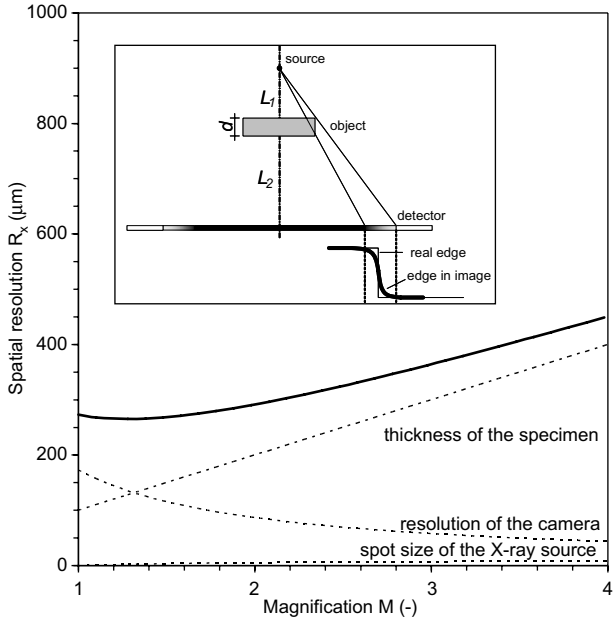

Fig. 2. Dependency of the spatial resolution on the magnification for the specific case where $L_1 + L_2 = 2000$ mm, $\sqrt{x^2 + y^2} = 10$ mm and $d = 10$ mm. The dotted lines represent the dependency on each of the three terms at the right hand side of Eq. (4): the spot-size of the X-ray source, the resolution of the detector and the thickness of the sample. The inset shows the influence of the thickness on the spatial resolution: the specimen edge is not seen as a jump on the detector, but as a smooth attenuation function, called the edge-response function (ERF).

This makes the spatial resolution R_x also function of the thickness of the specimen d and of the position in the specimen. It can be approximated as:

$$R_x = \frac{R_d}{M} + \left(1 - \frac{1}{M}\right) l_s + \frac{(M-1) \cdot d \cdot \sqrt{x^2 + y^2}}{L_2} \tag{4}$$

The first term at the right hand side corresponds to the dependency on the resolution of the detector, the second term to the influence of the spot size and the last term to the influence of the specimen thickness, in which $\sqrt{x^2 + y^2}$ denotes the distance out of the centre of the X-ray beam. Fig. 2 illustrates the dependency of the spatial resolution on the three terms at the right hand side of Eq. (4) for the specific case where $L_1 + L_2 = 2000$ mm, $\sqrt{x^2 + y^2} = 10$ mm and $d = 10$ mm. It is obvious that a higher magnification now no longer increases the spatial resolution, but that an optimal magnification can be found depending on the different parameters. All measurements showed in this paper are performed with a magnification of 1.28. In this way the spatial resolution varies between 137 µm and 850 µm depending on the position in the specimen.

3. Quantification of moisture transfer using the X-ray projection technique

3.1. Measurement principle

For simplicity, the procedure for measuring moisture content profiles by means of X-ray radiography is explained for a capillary uptake experiment. In this experiment an oven dry plate ($h \cdot l \cdot d$) absorbs liquid water at the bottom side ($l \cdot d$) from a free water plane. First an X-ray image of the oven-dry plate is taken. Then during

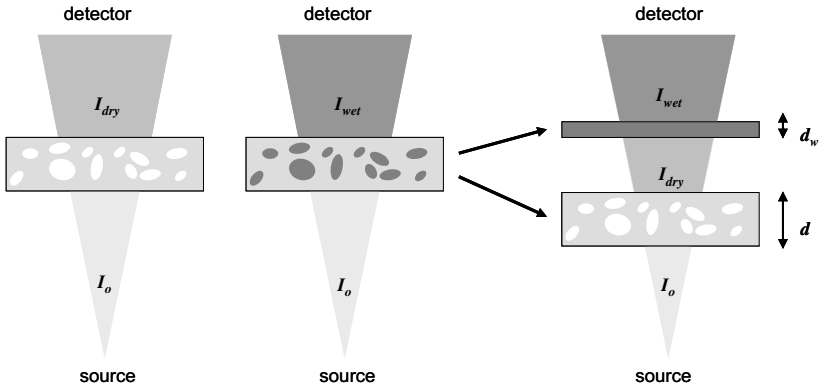

Fig. 3. The moisture distribution is obtained by logarithmically subtracting an image of the dry sample I_{dry} from an image of the wet sample I_{wet}. The attenuation due to the liquid water in the porous material can be seen as the attenuation by a fictitious layer of liquid water with thickness d_w placed behind the dry sample.

the uptake process, images of the wet plate are taken at regular time steps. According to Eq. (1), the transmitted X-ray intensity I through the dry and wet plate are:

$$I_{dry} = I_0 \exp(-\mu d) \tag{5}$$

$$I_{wet} = I_0 \exp(-\mu d - \mu_w d_w) \tag{6}$$

with μ and μ_w the attenuation coefficients of respectively the dry material and liquid water (index w) and d the thickness of the plate. The thickness d_w has to be read as the thickness of a fictitious water layer in agreement with the water content in the material. This concept is schematically depicted in Fig. 3.

The moisture content w (kg/m^3) is defined as:

$$w = \frac{\rho_w V_w}{V} = \frac{\rho_w d_w}{d} \tag{7}$$

with V the volume of the sample, V_w the volume of water and ρ_w the density of water. Using Eq. (7), we rewrite Eq. (6) as:

$$I_{wet} = I_{dry} \exp\left(-\frac{\mu_w w d}{\rho_w}\right) \tag{8}$$

and get the following expression for the moisture content:

$$w = -\frac{\rho_w}{\mu_w d} \ln\left(\frac{I_{wet}}{I_{dry}}\right) = -\frac{\rho_w}{\mu_w d}(\ln(I_{wet}) - \ln(I_{dry})) \tag{9}$$

The equation indicates that the moisture content at each position can be quantified by logarithmically subtracting the reference image of the dry sample from the images of the wet sample.

3.2. Moisture content resolution R_w

We use a 12 bit CCD-camera with 4096 grey levels. The resolution in moisture content R_w is defined as the moisture content corresponding to one greyscale difference between I_{wet} and I_{dry} or according to Eq. (9):

$$R_w = -\frac{\rho_w}{\mu_w d} \ln\left(\frac{I_{dry} - 1}{I_{dry}}\right) \tag{10}$$

Note that when we refer to a high resolution in moisture content, a low value of R_w is indicated. We observe in Eq. (10) that the resolution R_w depends on the properties of the liquid (the density ρ_w and attenuation coefficient μ_w), the sample thickness d and the intensity I_{dry}. Because of the latter (according to Eqs. (2) and (3)), R_w further depends on material dependent parameters (effective atomic number Z_e and material density ρ) and the energy of the source E. This means that for each material and liquid, a sample thickness d_{opt} and X-ray energy E_{opt} can be determined which optimise the moisture resolution (minimal value for R_w).

3.3. Optimal specimen thickness and optimal energy

We determine the optimal parameters d_{opt} and E_{opt} for two materials with different density: ceramic brick ($\rho =$ 2001 kg/m^3, $Z_e \approx 11.92$) and calcium silicate board ($\rho =$ 270 kg/m^3, $Z_e \approx 15.80$). Ceramic brick is made of fired homogenised clay, whereas calcium silicate board is largely composed of synthetic mineral xonotlite [16]. As liquid, we used demineralised water ($\rho_w = 1000$ kg/m^3). Based on Beer's law (Eq. (1)) the attenuation coefficient can be obtained by measuring the logarithmic difference between incident and transmitted X-ray intensity $\ln(I_{dry}/I_0)$. The intensity I_0 is determined by taking an image of the empty space. Fig. 4 shows the measurements of $\ln(I_{dry}/I_0)$ for water, ceramic brick and calcium silicate board as function of the thickness at a source energy of 50 keV. If Eq. (1) holds a linear relationship has to be found, where the slope of the regression line corresponds to the attenuation coefficient. As can be seen in Fig. 4, water obeys Beer's law, whereas for ceramic brick a strong non-linear behaviour is observed. The non-linear behaviour can be explained by the polychromatic nature of the X-rays. The X-ray energy spectrum is shown in Fig. 5(a). When a polychromatic X-ray beam passes through an object, low energy photons are more rapidly absorbed than photons of higher energy. Hence the spectrum is unequally filtered and gradually changes (see Fig. 5(a)). This phenomenon, where the

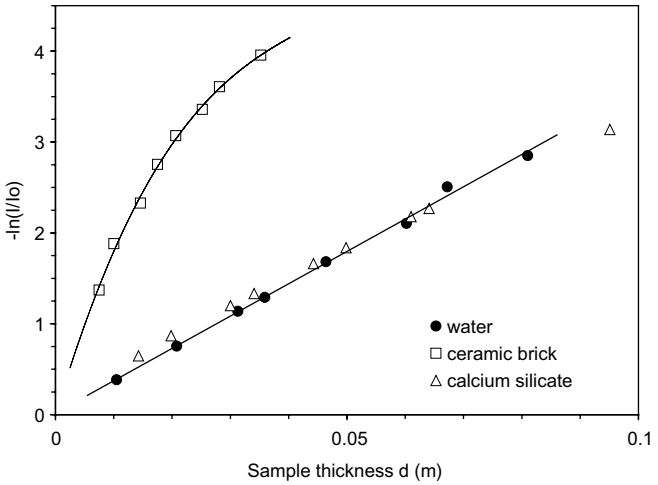

Fig. 4. Determination of the attenuation coefficients of water, ceramic brick and calcium silicate plate for a source energy of 50 keV.

X-ray beam gradually becomes *harder* (i.e. the mean energy increases) is known as beam hardening [17]. Eq. (2) indicates that the attenuation coefficient decreases when the mean energy increases. As a result the $\ln(I_{dry}/I_0)$ curve will gradually deviate from the straight line with increasing thickness of the specimen (Fig. 5(b)). Fig. 4 shows that beam hardening is more pronounced in denser materials (ceramic brick) compared to low density materials (calcium silicate). In this case an effective attenuation coefficient $\mu_{ef} = \mu(d)$ for a specimen with constant thickness d can be determined (see Fig. 5(b)). The determination of attenuation coefficient and its dependence on thickness is repeated for different energy levels E. Based on the knowledge of the intensity I_0 as function of E and the attenuation coefficients μ and μ_w as a function of thickness and energy, we can calculate according to Eqs. (5) and (10), the moisture resolution R_w. Fig. 6 shows R_w versus the sample thickness d for different source energies E. For every energy level, a minimal R_w can be found. The minimum in the curve gives the optimal thickness d_{opt}. We observe that the optimal thickness shifts to higher values with increasing energy. For ceramic brick the optimal thickness varies between 6 mm ($E = 50$ keV) and 13 mm ($E = 85$ keV). For the low density material calcium silicate the optimal thickness varies between 40 mm ($E = 70$ keV) and 60 mm ($E = 100$ keV). In Fig. 7 the moisture resolution R_w versus energy is given for a ceramic brick sample with optimal thickness d_{opt}. It is clear that increasing the source energy results in a better resolution in moisture content (decreasing value of R_w). For comparison we also give the moisture resolution for a specimen with constant thickness of 20 mm (higher than the optimal thickness). For high energy levels, the resolution for the specimen with constant thickness does not deviate much from the resolution at optimal thickness. These observations are in favour of choosing high energies. However, the X-ray source proved to become unstable at high voltages ($\geqslant$100 keV). Also the object in the apparatus warms up during radiation with high energies (resulting in an increase of possible evaporation at top and lateral sides). Fig. 7 shows that the improvement of moisture resolution levels off at higher energies (>90 keV). Therefore, it is reasonable to choose an energy level of 85 keV, which showed to be a good compromise between stability of the source and resolution in moisture content.

At $E = 85$ keV, the optimal sample thickness is 50 mm for calcium silicate and 13 mm for ceramic brick, with corresponding moisture content resolution R_w of respectively 0.8 kg/m^3 and 3.2 kg/m^3.

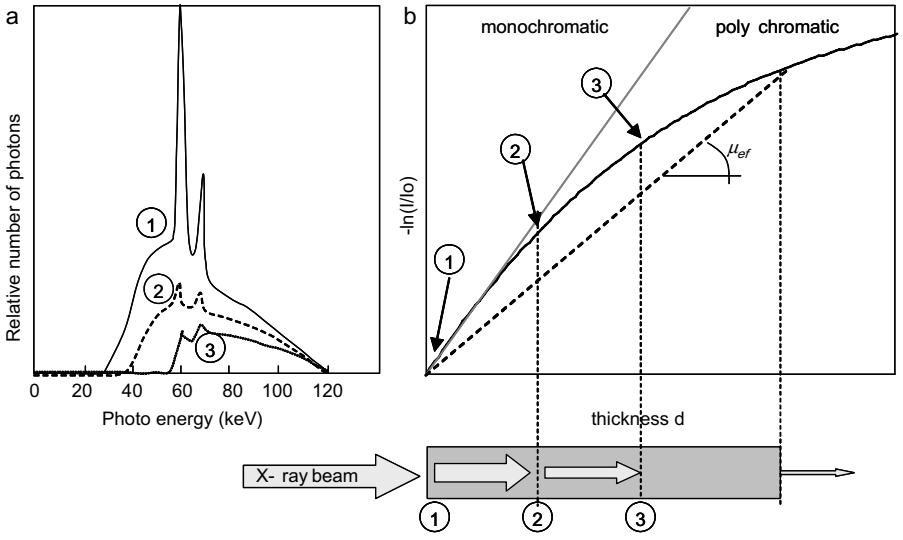

Fig. 5. (a) The beam hardening effect. When a polychromatic beam passes through an object, the initial spectrum (curve 1) is unequally filtered and changes to the curves 2 and 3. (b) The beam hardening effect explains the non-linearity of $-\ln(I_{dry}/I_0)$ as a function of the specimen thickness. For a constant thickness of the specimen an effective attenuation coefficient μ_{ef} is used.

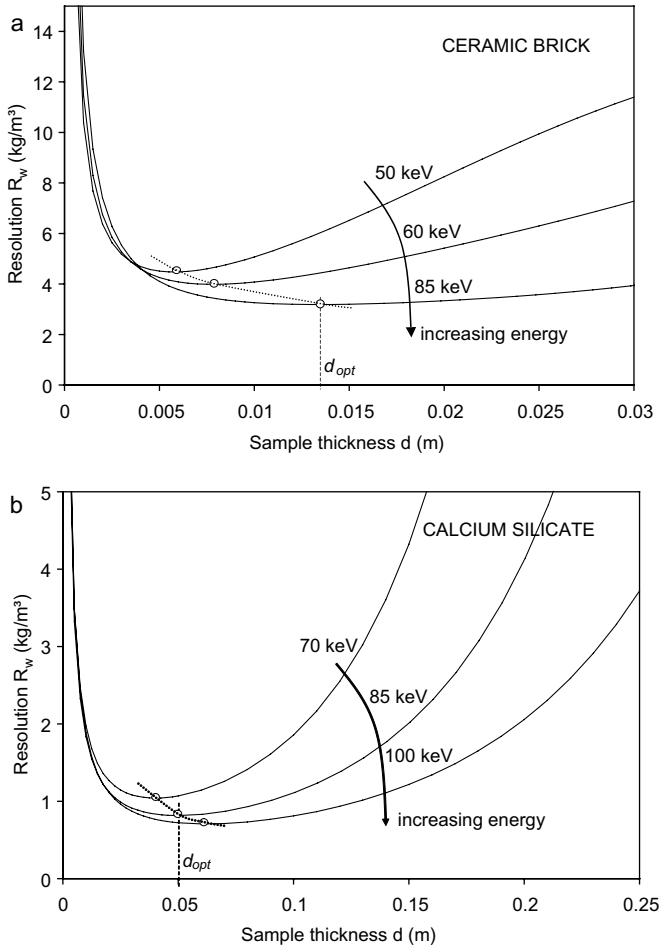

Fig. 6. Calculated resolution in moisture content R_w as a function of sample thickness and energy of the X-ray source: (a) ceramic brick, (b) calcium silicate plate. The minimum indicates the optimal sample thickness.

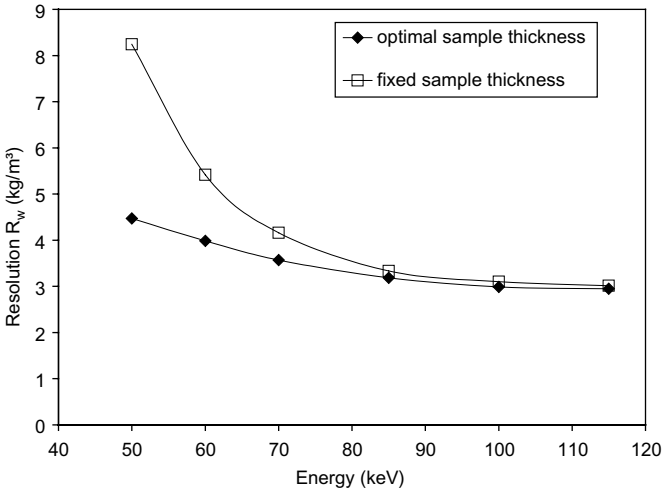

Fig. 7. Moisture resolution R_w versus the source energy for ceramic brick. The resolution for a specimen with optimal thickness for every energy level is compared with a specimen with constant thickness ($d = 20$ mm).

3.4. Determination of 1D-moisture profiles during a liquid water uptake experiment

Following the procedure explained in 3.1, we determine the moisture content distribution in a sample of calcium silicate board ($70 \times 60 \times 30\ \text{mm}^3$) during a liquid water uptake experiment. Fig. 8 (bottom) shows the moisture content distribution in the board (uptake in the x-direction) as a greyscale map (pixel size of 137 μm). The moisture content shown is a value averaged over the thickness. We observe the moisture front to be almost uniform showing the material to be homogeneous. However, when comparing in detail moisture content profiles $w(x)$ along the x-axis at neighbouring y positions, we observe small differences between the different profiles. The scatter is due to random measurement errors and the small scale heterogeneity of the material. To reduce scatter, we average neighbouring $w(x)$-profiles over a zone of n pixels wide ($\Delta y = nR_d/M$). The zone is situated in the middle of the

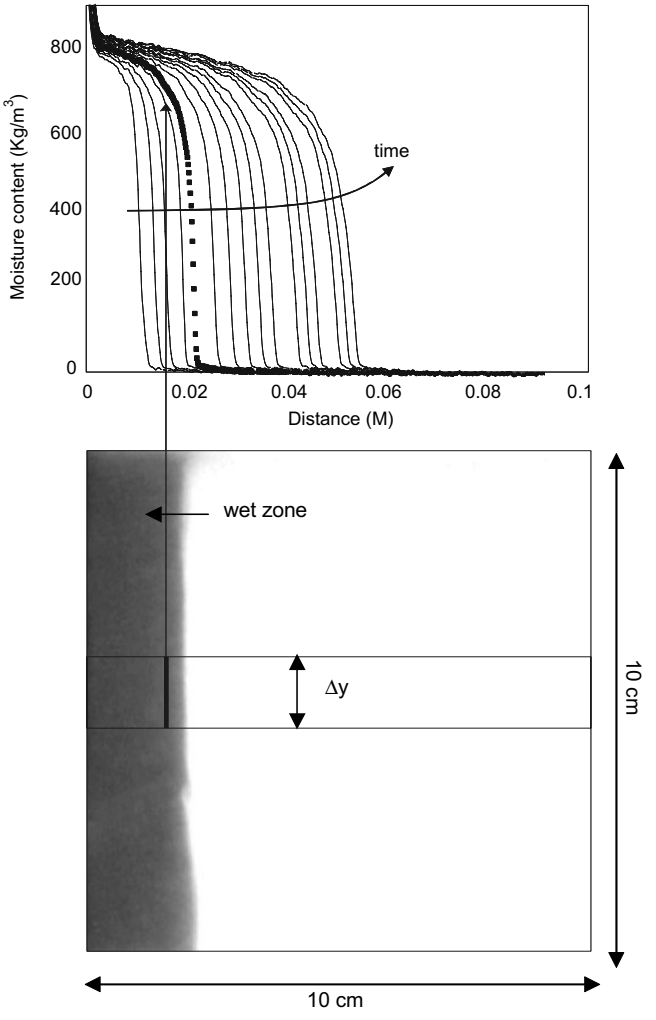

Fig. 8. Top: moisture content profiles at different time steps during capillary water uptake in calcium silicate plate. The profiles are determined from a two-dimensional moisture content map (bottom) by averaging over a zone Δy. The capillary uptake is from the left side.

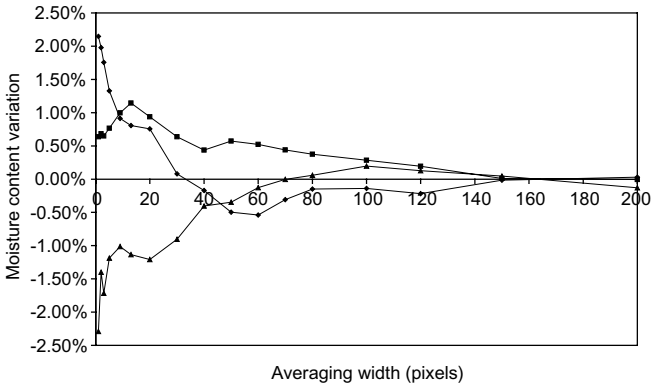

Fig. 9. The fluctuations of the relative variation of the average moisture content at three positions x_i (Fig. 8 bottom) as function of the number of averaging pixels.

specimen (Fig. 8 bottom). Fig. 9 gives the relative variation of the average moisture content at three positions x_i as a function of the averaging width Δy. It is defined as

$$s_w = \frac{w_{\Delta y, x_i} - \bar{w}_{x_i}}{\bar{w}_{x_i}} \tag{11}$$

with $w_{\Delta y, x_i}$ the averaged moisture content over the zone Δy and $\bar{w}_{x_i}$ the mean moisture content at x_i (averaged over the total width of the sample). We observe that the fluctuations gradually fade away with increasing bandwidth. For the case presented the relative variation is less than $\pm 1\%$ once $\Delta y > 3$ mm ($n = 22$ pixels). This means that the small scatter can be easily filtered out without information loss on e.g. material heterogeneity. Fig. 8 (top) gives the evolution in time of the characteristic moisture content profiles determined by the averaging method ($n = 20$) described above.

This analysis shows that the X-ray projection method is a fast two-dimensional method, which takes about 10 s to determine the moisture content with a high moisture content resolution (3.2 kg/m^3 for ceramic brick and 0.8 kg/m^3 for calcium silicate plate). This high moisture content resolution is achieved at the optimal thickness of the specimen (13 mm and 50 mm for respectively ceramic brick and calcium silicate board). Remember that the thickness of the plate also influences the spatial resolution. This drawback is more pronounced further away from the centre of the X-ray beam. So, the thickness of a specimen should be chosen based on the overall dimensions of the plate and the desired moisture content resolution.

4. Analysis of two-dimensional liquid water uptake in homogeneous, heterogeneous, micro- and macro fractured materials

We illustrate the applicability of the X-ray projection method by measuring two-dimensional liquid water uptake in homogeneous, heterogeneous, micro- and macro-fractured materials. In particular, we analyse the validity of a moisture diffusion approach. Based on the conservation of mass and assuming Darcy's law for liquid water transfer, one-dimensional isothermal liquid water transfer can be formulated with a one-phase diffusion equation

$$\frac{\partial w}{\partial t} = \frac{\partial}{\partial x}\left(D(w)\frac{\partial w}{\partial x}\right) \tag{12}$$

with the moisture content w as the governing variable and $D(w)$ the liquid water diffusivity, which is only dependent on the moisture content. Boltzmann (1894, cited in Crank [18]), showed that for water uptake in a semi-infinite homogeneous and isotropic specimen with constant initial moisture content w_0 ($w = w_0$ at $x > 0$ and $t = 0$) and constant moisture content w_B at the water uptake side ($w = w_B$ at $x = 0$ and $t > 0$), the differential Eq. (12) has one unique solution. This solution is called the characteristic curve or w–λ profile, where the Boltzmann variable λ is defined as $\lambda = x/\sqrt{t}$. This means that when moisture content profiles measured at different time steps are subjected to a Boltzmann transformation, all transformed data should coincide to form a single curve. We will use the Boltzmann transformation technique to evaluate the validity of Eq. (12).

4.1. Homogeneous material: calcium silicate brick

Fig. 10 shows the transformed w–λ data set corresponding to moisture content profiles of Fig. 8. The transformed data coincide within a small band of the scatter forming a single well-defined curve, which indicates the diffusion Eq. (12) to be valid. However, some discussion is appropriate concerning the particular shape of the w–λ profile. The w–λ profile consists of three zones: a small boundary layer with high moisture contents (zone I), a transition zone with a rather constant moisture content (zone II), and a steep wetting front (zone III). The movement of the steep wetting front as well as the liquid water transport in the transition zone II is primarily governed by capillary forces, that validates a one-phase diffusion approach. During this capillary absorption process, air initially present in the pores

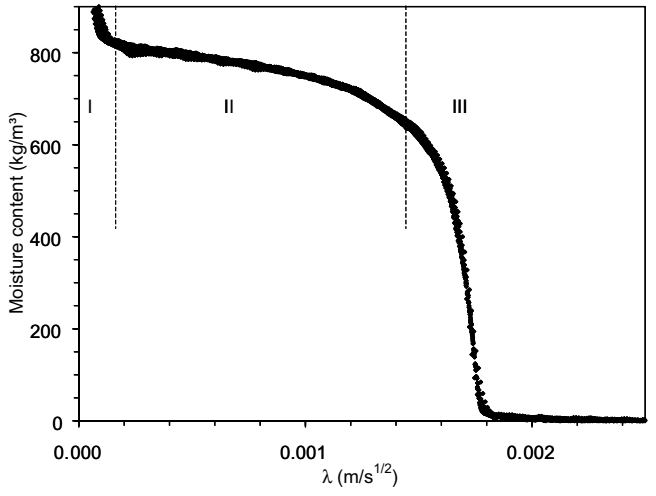

Fig. 10. Moisture content versus Boltzmann-variable λ after transforming the data of Fig. 8 (Calcium silicate board).

is partly entrapped, preventing absorption until full saturation [19]. Only at the water/specimen interface ($x = 0$) full saturation is attained. The further water absorption process in zone I is predominantly determined by diffusion of entrapped air through the partly water filled pore system. Due to air diffusion, the saturation front moves inwards from the water/specimen boundary following a square root of time relation, but compared to the capillary absorption process this process is much slower. The transformed data in the boundary zone therefore converge approximately into one curve, although the one-phase water diffusion approach (Eq. (10)) does not strictly apply in this zone. We note that the moisture diffusivity can be determined from this w–λ profile using adequate smoothing techniques [20].

4.2. Heterogeneous material: ceramic brick

Ceramic brick is a fired machine-moulded brick made from homogenised clay, but which shows due to the manufacturing process an inherent small-scale heterogeneity. The sample used has overall dimensions of $70 \times 70 \times 20\ \text{mm}^3$. Fig. 11(a) shows the measured moisture content profiles as determined by the procedure proposed in 3.3 ($\Delta y =$ 2 mm). The moisture content profiles show high variations. The form of the different profiles (the position of local maxima and minima) however reproduces for different points in time. The variations thus reflect inhomogeneity present in the sample. Fig. 11(b) gives the transformed w–λ profile. We observe that early measured data (<120 s) fall out of the characteristic band. The measured data after this initial period converge into a wide band of random scatter without a systematic time tendency. The material thus obeys, on an average sense, the diffusion equation except for its initial period. The anomalous behaviour in the initial phase may be caused by the following phenomena. First, non-ideal one dimensional water contact conditions may exist. We mention the presence of a slight hydrostatic overpressure due to immersion of the specimen in water (immersion depth of around 2 mm) and the three dimensional flow in a small boundary layer due to the presence of a water meniscus at the lateral sides of the specimen in contact with water. Second, the presence of small-scale inhomogeneities and irregularities such as small microcracks in the contact layer may result in preferential wetting during the initial phase. With ongoing time, liquid water redistribution in the y-direction of the specimen becomes more important and results in a flattening of the moisture front at subsequent time intervals.

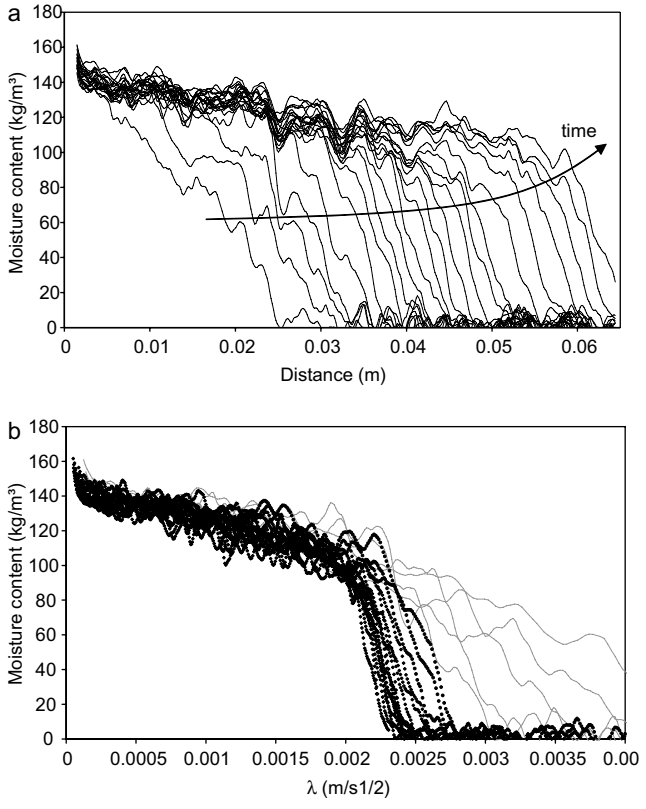

Fig. 11. (a) Moisture content profiles at different time steps during capillary water uptake in ceramic brick. (b) Moisture content versus Boltzmann-variable λ after transforming the data of Fig. 11(a). The grey lines represent transformed moisture profiles at the early stage of the absorption process (<120 s) and fall out of the band of the characteristic curve (black dots).

4.3. Micro-fractured material: cellular concrete

In a third example we investigate liquid water uptake in autoclaved aerated concrete (AAC). The pore structure of AAC is unusual in having a well-defined bimodal pore size distribution. The material has a micro-capillary pore system (±0.1 μm) between plate-shaped needle crystals of the cementitious matrix, within which are dispersed large aeration pores formed by foaming the wet slurry during manufacture. The aeration pores are coarse (diameter typically 0.1–1.0 mm). The connectivity of the aeration pores is not well understood, although since they are formed as bubbles within the matrix they may be presumed to be connected mainly via the finer matrix pores. Roels et al. [21] showed that a limited number of macro-capillary pores (10 μm) connect the air bubbles, which may play an important role in the moisture transport process. The sample has overall dimensions of $52 \times 48 \times 25\ \text{mm}^3$. The evolution of the moisture distribution with time is given in Fig. 12. Fig. 12(a) clearly shows that in the initial stage, the moisture front is not uniform due to preferential wetting patterns. Detailed analysis showed that the preferential wetting patterns are caused by the presence of macro-pores and micro-cracks interconnecting several aeration pores, which may considerably accelerate the water uptake compared to the water transport in the bulk material. The micro-cracks can originate from the production process (cracking due to drying shrinkage) or from the specimen preparation (cutting and drying). The crack width is in the order of 0.1 mm. We may assume that micro-cracks do not completely interconnect, since preferential wetting

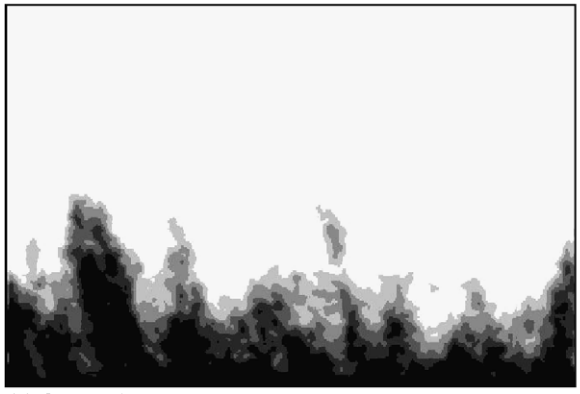

(a) 2 min 5 sec

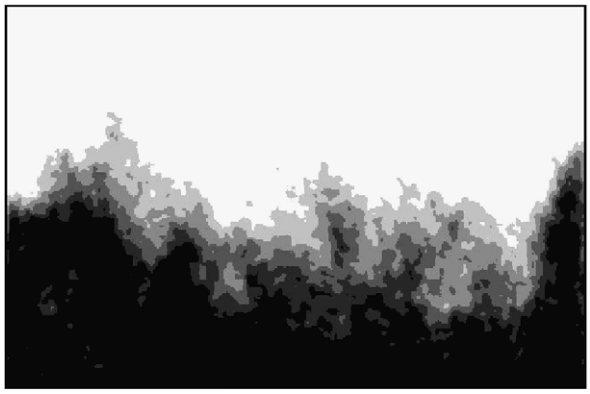

(b) 7 min 20 sec

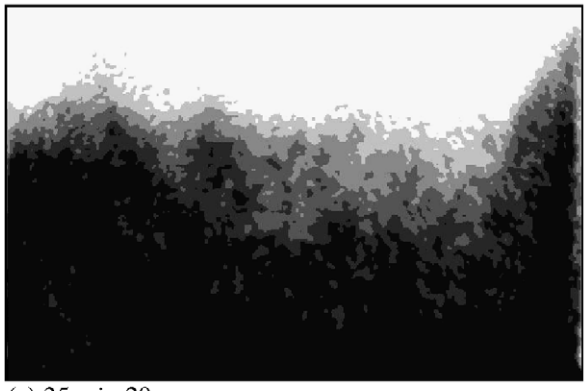

(c) 35 min 20 sec

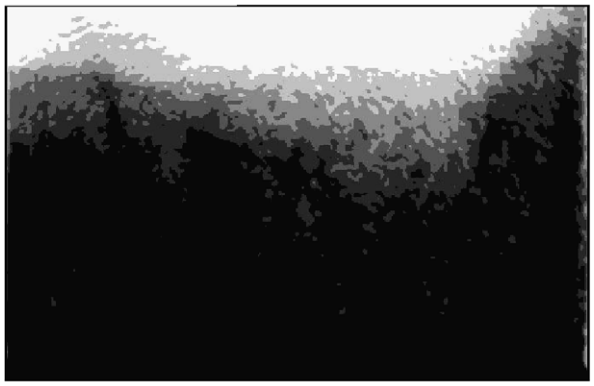

(d) 78 min 20 sec

Fig. 12. Images of the two-dimensional moisture distribution in micro-fractured cellular concrete during capillary water uptake from the bottom side. The baseline of each image measures 52 mm.

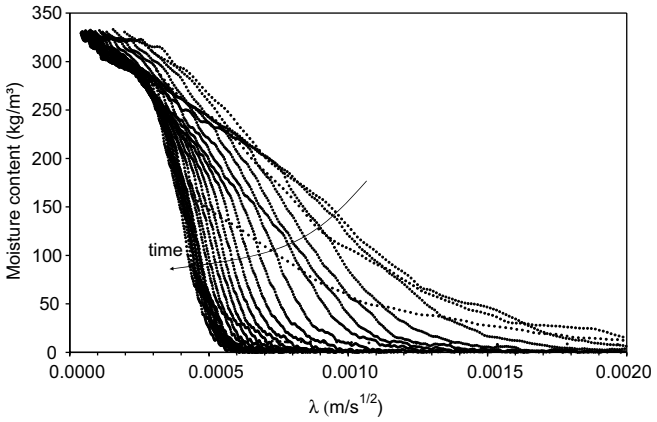

Fig. 13. Moisture content versus Boltzmann-variable λ after transforming moisture content profiles of micro-fractured AAC. The transformed data do not converge into a single curve.

gradually slows down in time. Fig. 12(b) shows that redistribution from the water-filled micro-cracks to the surrounding matrix seems to result in a flattening of the moisture front at subsequent time intervals (see Figs. 12(c) and (d)). Fig. 13 shows the Boltzmann transformation of the measured data. It is clear that due to the specific pore structure of AAC and the presence of microcracks, the transformed data do only converge into a single curve after a long period. This indicates that a single diffusivity $D(w)$ as proposed in Eq. (12) seems only appropriate to describe liquid water transport in micro-fractured AAC for water absorption processes lasting longer than an hour.

4.4. Macro-fractured material

In a last example, we analyse free water uptake in a fractured brick sample with a macro-crack. The specimen measures $80 \times 80 \times 20$ mm^3. To create a 'natural' (i.e. not made by saw cutting) fracture, the sample was broken and afterwards reassembled resulting in an average crack width of 0.1 mm. Fig. 14 gives the evolution in time of the moisture distribution. The figures clearly show a rapid preferential wetting of the material around the crack. Afterwards, the fracture acts as an extra water source for the surrounding matrix over the total height of the specimen. Besides the moisture distribution in the ceramic brick also the water filled part of the fracture is visible. The waterfront in the fracture quickly reaches the opposite side of the specimen. As can be seen on the bottom image, the final moisture distribution is somehow asymmetric. Liquid water flow from the fracture to the matrix at the right side of the fracture seems to be obstructed by the presence of a small secondary crack running parallel to the main fracture.

5. Conclusions

X-ray projection is proposed as a fast and accurate method for the non-destructive determination of two-dimensional moisture distributions in porous materials.

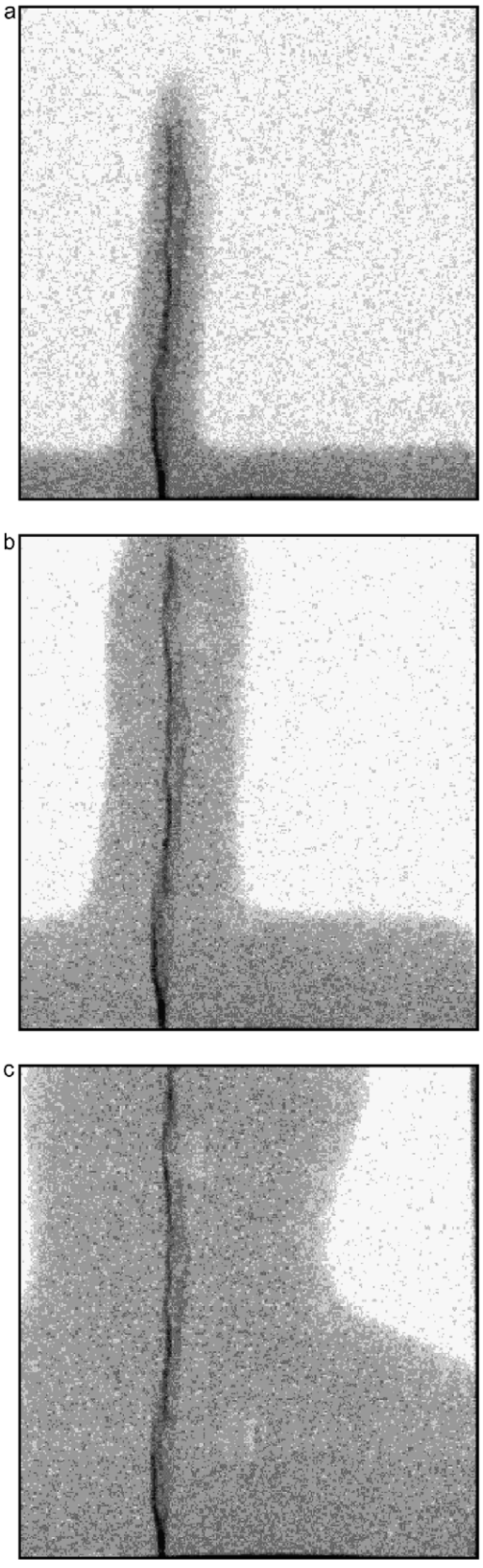

Fig. 14. Two-dimensional images of water uptake in a naturally fractured brick sample after 33 s (a), 2 min 30 s (b) and 10 min (c). The fracture aperture is around 0.1 mm.

The quantitative determination of the moisture content is based on the logarithmic subtraction of a reference image (e.g. sample at dry state) from images of the wet sample. The resolution in moisture content can be optimized choosing an appropriate thickness and energy of the X-ray source. The optimal thickness depends on the material used and increases with the energy of the X-ray source.

Compared to common techniques as NMR and gamma-ray, the X-ray method has the advantage that two-dimensional images are directly obtained with good resolution in space, time and moisture content. The two-dimensionality and high resolution characteristics make the method extremely useful for the analysis of transient moisture flow in homogeneous, heterogeneous, micro- and macro-cracked materials. Based on the Boltzmann transformation method we studied the validity of a one-phase water diffusion approach. Micro- and macro-cracked porous materials do not obey the diffusion equation with a diffusivity only dependent on moisture content. For homogeneous and small-scale heterogeneous materials the one-phase diffusion approach is found to be valid.

Applying computer tomography (μCT) an extension of the proposed method can be made to three dimensions, that makes the technique extremely suitable to determine successive moisture content distributions in space and time in composite and heterogeneous porous media.

Acknowledgements

Part of the work described in this paper has been performed within KUL OT/04/28 'Towards a reliable prediction of the moisture stress on building enclosures', funded by the K.U. Leuven. This financial support is gratefully acknowledged. All measurements with the X-ray radiography equipment were performed at the Department of Metallurgy and Materials Engineering of the K.U. Leuven. We would like to thank Prof. dr. ir. M. Wevers and her co-workers for the fruitful collaboration.

References

[1] H. Ferguson, W.H. Gardner, Diffusion theory applied to water flow data obtained by gamma ray absorption, Soil Science Society of America Proceedings 27 (1963) 243–246.
[2] A. Nielsen, Gamma-ray attenuation used for measuring the moisture content and homogeneity of porous concrete, Building Science 7 (1972) 257–263.
[3] M.K. Kumaran, M. Bomberg, A gamma-spectrometer for determination of density distribution and moisture distribution in building materials, in: Proceedings of the International Symposium on Moisture and Humidity, Instrument Society of America, Washington DC, 1985, pp. 485–490.
[4] F.J. Gummerson, C. Hall, W.D. Hoff, R. Hawkes, G.N. Holland, W.S. Moore, Unsaturated water flow within porous materials observed by NMR imaging, Nature 281 (1979) 56–57.
[5] L. Pel, Moisture transport in porous building materials, Ph.D. thesis, TU/e, Eindhoven, Netherlands, 1995.
[6] I.V. Mastikhin, B. Mullally, B. MacMillan, B.J. Balcom, Water content profiles with a 1D centric SPRITE acquisition, Journal of Magnetic Resonance 156 (2002) 122–130.

[7] Q. Chen, M.K. Gingras, B.J. Balcom, A magnetic resonance study of pore filling processes during spontaneous imbibition in Berea sandstone, Journal of Chemical Physics 119 (2003) 9609–9616.
[8] B. Masschaele, M. Dierick, V. Cnudde, L. Van Hoorebeke, S. Delputte, A. Gildemeister, R. Gaehler, A. Hillenbach, High-speed thermal neutron tomography for the visualization of water repellents, consolidants and water uptake in sand and lime stone, Radiation Physics and Chemistry 71 (2004) 807–808.
[9] T. Cadoret, D. Marion, B. Zinszner, Influence of frequency and fluid distribution on elastic wave velocities in partially saturated limestones, Journal of Geophysical Research 100 (B6) (1995) 9789–9803.
[10] V. Tidwell, L. Meigs, T. Christian-Frear, C. Boney, Effects of spatially heterogeneous porosity on matrix diffusion as investigated by X-ray absorption imaging, Journal of Contaminant Hydrology 42 (2000) 285–302.
[11] S. Akin, J.M. Schembre, S.K. Bhat, A.R. Kovscek, Spontaneous imbibition characteristics of diatomite, Journal of Petroleum Science and Engineering 25 (2000) 149–165.
[12] G.F. Knoll, Radiation Detection and Measurement, J. Wiley, 1989.
[13] M. Van Geet, Optimisation of microfocus X-ray computer tomography for geological research with special emphasis on coal components and fractures characterisation, Ph.D. thesis, KULeuven, Leuven, Belgium, 2001.
[14] S.L. Wellington, H.J. Vinegar, X-ray computerized tomography, Journal of Petroleum Technology (August) (1987) 885–898.
[15] D. Mouze, X-ray microradiography, in: S. Amelincks, D. Van Dyck, J. Van Landuyt, G. Van Tendeloo (Eds.), Handbook of Microscopy, I, VCH, Weinheim, 1996, pp. 130–147.
[16] A. Hamilton, C. Hall, Physicochemical characterisation of a hydrated calcium silicate board material, Journal of Building Physics 29 (1) (2005) 9–19.
[17] R.A. Brooks, G. Di Chiro, Beam hardening in X-ray reconstructive tomography, Physics in Medicine and Biology 21 (1976) 390–398.
[18] J. Crank, The Mathematics of Diffusion, University Press, Oxford, 1989.
[19] F. Descamps, Continuum and discrete modelling of isothermal water and air transfer in porous media, Ph.D. thesis, KULeuven, Leuven, Belgium, 1997.
[20] J. Carmeliet, H. Hens, S. Roels, O. Adan, H. Brocken, R. Cerny, Z. Pavlik, C. Hall, K. Kumaran, L. Pel, Determination of the liquid water diffusivity from transient moisture transfer experiments, Journal of Thermal Envelope and Building Science 7 (4) (2004) 277–306.
[21] S. Roels, J. Sermijn, J. Carmeliet, Modelling unsaturated moisture transport in autoclaved aerated concrete: a microstructural approach, in: A. Gustavsen, J.V. Thue (Eds.), Proceedings of the 6th Symposium on Building Physics in the Nordic Countries, Norwegian University of Science and Technology, Trondheim, Norway, 2002, pp. 167–182.